View metadata, citation and similar papers at core.ac.uk

brought to you by CORE

provided by Kanazawa University Repository for Academic Resources

Determining the relative permeability and conductivity of thin materials

著者	Yagitani Satoshi, Tosaka T., Nagano I., Yoshimura Y.
journal or publication title	IEEE TRANSACTIONS ON ELECTROMAGNETIC COMPATIBILITY
volume	47
number	2
page range	352-360
year	2005-05-01
URL	http://hdl.handle.net/2297/1818

Determining the Relative Permeability and Conductivity of Thin Materials

Toshihide Tosaka, *Student Member, IEEE*, Isamu Nagano, Satoshi Yagitani, and Yoshiyuki Yoshimura

***Abstract*—In order to determine the relative permeability and conductivity of thin materials that could not be found using traditional methods, we constructed a shield box and developed a measuring system to estimate the unknown electric parameters of exotic shielding materials such as thin cloths. Thin electromagnetic shielding sheets of both nonmagnetic materials and ferromagnetic materials were used. The shielding effectiveness of the materials was measured as a function of frequency, and the results were compared with the calculated solutions for a multilayered model that was evaluated using the Sommerfeld integral that expresses near-field spherical waves by a composition of cylindrical waves. In these calculations, the relative permeability and conductivity were varied to determine the solution closest to the measured results. The least squares method was used to determine the best fitted values. Initially the nominal values of relative permeability were assumed, and the conductivity was found using the fitting technique. Then this determined value of the conductivity was assumed, and the relative permeability was found using the fitting technique. For the nonmagnetic materials, the estimated relative permeability was the same as the nominal values. For the ferromagnetic materials, the estimated relative permeability varied 0%–30% from the nominal values. For both types of materials, the estimated conductivities were 0%–9.8% different from nominal values. This research details a new method for evaluating the attenuation of interfering electromagnetic waves for thin materials.**

***Index Terms*—Conductivity, electric parameters, estimation, relative permeability, shielding effectiveness, Sommerfeld integral.**

I. Introduction

RECENTLY, the use in everyday life of computers, mobile phones, PDAs, and many other electronic devices has increased dramatically. The use of electromagnetic waves in the technology of electronics and communications is being driven by the demand for these devices which today are essential for our economic and social life. It has been shown that electromagnetic waves leaking from electronic devices may cause incorrect operation of other electronic devices [1]. Experimental research and epidemiological research on the possible influence of electromagnetic waves on the human body has led to the establishment of guidelines for limiting exposure to time-varying electric, magnetic, and electromagnetic fields [2].

If external interfering waves are sufficiently attenuated by a device, they will not cause problems with the operation of the device. Over the years, shielding materials have been developed to attenuate these interfering electromagnetic waves. The objects with the greatest shielding effectiveness (SE), the measured attenuation of the interfering electromagnetic waves, were metallic plates. But today, after many advancements in the development of plating technology have occurred, metals can now be plated onto thin cloths. The demand is increasing for electromagnetic shielding cloths which cover the electronic devices and which are light and strong.

For attenuating an interfering wave, we have to attenuate 30 dB or more using shielding materials [3]. For attenuation we usually use thick materials, but for many applications the use of thick materials is unrealistic. In these situations, using materials with a thickness of less than 1 mm is more realistic. We focus our attention on the low frequency range (1 MHz and below), because many items of electrical equipment today use electromagnetic waves in that range. For the low frequency range, it is relatively easy to use shielding materials to attenuate electric fields, but it is difficult to attenuate magnetic fields. In order to effectively attenuate magnetic fields in the low frequency range, we must investigate the propagation mechanism of the electromagnetic waves by using numerical analyzes [4], [5]. First, we specify the SE desired at a given frequency, and then we determine the electric parameters required to realize that SE. Using the electric parameters, we can easily develop a shielding sheet which has the desired attenuation. These results should be considered in the design of shielding materials. It is important to know about the electric parameters (relative dielectric constant ε_r, relative permeability μ_r, conductivity σ), because they determine the attenuation of an electromagnetic wave. Methods exist to measure the relative permeability and conductivity of many materials. For most uniform solid materials, the standard way to determine permeability is by generating a $B-H$ curve, and the standard way to measure the conductivity is by using a four-point probe array. But if the materials are thin cloths, such testing would be difficult and the results could be erratic. Another method has been developed to measure the magnetic properties of steel sheets and strips through the use of an Epstein frames described in [6] and [7]. Four quarter sections of toroidal coils contain the primary and secondary windings around the square frame core made of overlapping sections of the test material. But the applicable frequency ranges are less than 10 kHz, and it is difficult to measure thin materials. An electromagnetic shielding sheet is plated and formed with many layers and many fibers which are less than 0.1 mm in diameter. Therefore, the surface of this sheet is uneven when observed on a microscopic scale. No estimation system exists for this case. Up to now,

Manuscript received January 15, 2004; revised September 11, 2004.

T. Tosaka, I. Nagano, and S. Yagitani are with the Graduate School of Natural Science and Technology, Kanazawa University, Ishikawa, Japan (e-mail: tosaka@reg.is.t.kanazawa-u.ac.jp).

Y. Yoshimura is with the Product and Technology Department, Industrial Research Institute of Ishikawa, Ishikawa, Japan.

Digital Object Identifier 10.1109/TEMC.2005.847397

0018-9375/$20.00 © 2005 IEEE

we have not been able to estimate the electric parameters for these materials, and their electric parameters have remained unknown.

To determine the electric parameters of thin shielding materials, we have measured the SE using a shielding box and fitted the results to the numerical calculations for a near-field electromagnetic wave [8]. By adjusting the electric parameters in the calculation until the best fit with the measured values was found, we were able to estimate the electric parameters. For the numerical calculations, we assumed that a magnetic dipole source was located vertically perpendicular to the material. Then, in consideration of the source, we used the Sommefeld integral that expresses spherical waves by composition of cylindrical waves [9]. Up to now, we have assumed that for the numerical calculations in the low frequency range, the estimated relative permeability was constant as a function of frequency. But in fact, this is only true for nonmagnetic materials. The relative permeability of ferromagnetic materials varies as a function of frequency. Not taking this into account leads to inaccurate results.

In this research, we measure as a function of frequency the SE of ferromagnetic materials and nonmagnetic materials which have known electric parameters. Then we estimate the relative permeability and conductivity by varying these parameters in calculating a theoretical SE and finding a best fit to the measured values. We then compare the values obtained by our method with the nominal values [10], [11]. So far, many of the nominal values were derived for the dc (direct current) case. They are not necessarily appropriate for ac (alternating current). The magnetic flux density may or may not be a linear function of the magnetic field, depending on the type of material or medium, and the permeability may or may not be constant [12] for magnetic materials. The relative permeability is determined from the environment and frequency of the measurement, and the different values of permeability is obtained for different frequencies. Thus, there are no data for the ac case of relative permeability. The estimation of relative permeability has not yet been established for the ac case. For the case of thin cloth, measurement is difficult and erratic. But, for solid metallic materials, both thick and thin, it is easy to measure relative permeability by generating a $B - H$ curve. Therefore, we measure $B - H$ curves for various metals as a function of frequency. From these we calculate a relative permeability at each frequency for each metal. We then compare the measured SE with the calculated values using these designated "nominal" values in order to confirm the validity of our method.

Prior to this research, there was no measurement system of SE for the low frequency range. But by using the shield box which we have developed, we can now measure SE in the low frequency range and estimate the relative permeability and the conductivity in the low frequency range at the same time.

II. Shield Box

A. Measurement Using a Shield Box

In this research, we developed a shielding box as shown in Fig. 1. The shield box is made of 3-mm thick copper (Cu) plate. The box can be separated into an upper part and a lower part. A loop antenna transmitter and a loop antenna receiver are located

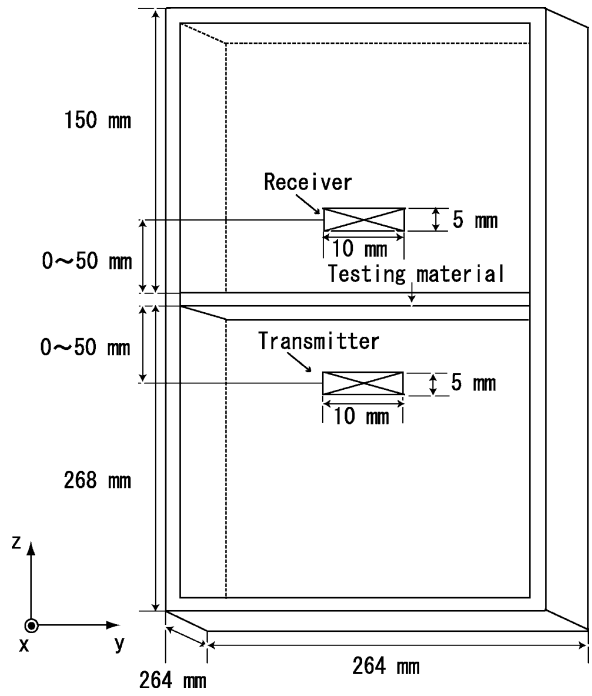

Fig. 1. Shield box.

in the lower part and the upper part of the box, respectively. The input signals to the loop antenna transmitter and the signals detected by the loop antenna receiver are measured using spectrum analyzers. The diameters of these antennas are 10 mm and the heights of the antennas' coils are 5 mm. The number of turns of the transmitter is 10, and the number of turns of the receiver is 500. The transmitter's current is 2.6 mA. The planes of the transmitter, receiver and testing material are parallel. The transmitter is directly below the receiver. Each of the transmitter and the receiver can move 0 to 50 mm away from the testing material. The testing material is placed between the upper and lower parts of the box. The SE is defined as the ratio of the magnetic field strength at the receiver without the testing material (H_0) to that with the testing material (H_1)

$$SE = 20 \log_{10} \frac{|H_0|}{|H_1|}. \tag{1}$$

B. Influence of Circumference of Shield Box

The shield box is constructed so that we can shield any noise coming from outside. If the transmitted magnetic field from the source leaks through the side panels of the shield box, we may not accurately find the SE of the testing material. Therefore, the influence of the circumference of the shield box is taken into consideration both in the computer simulation and in the actual experimental measurements.

We use a software program named MAFIA which can numerically calculate an electromagnetic field [13]. The basis of all simulations is the theory of the discrete Maxwell grid equations, the so called finite integration technique (FIT), which has been developed during the last twenty years. FIT is closely related to the finite-difference time-domain (FDTD) method, although the former is more general as in addition to the time domain,

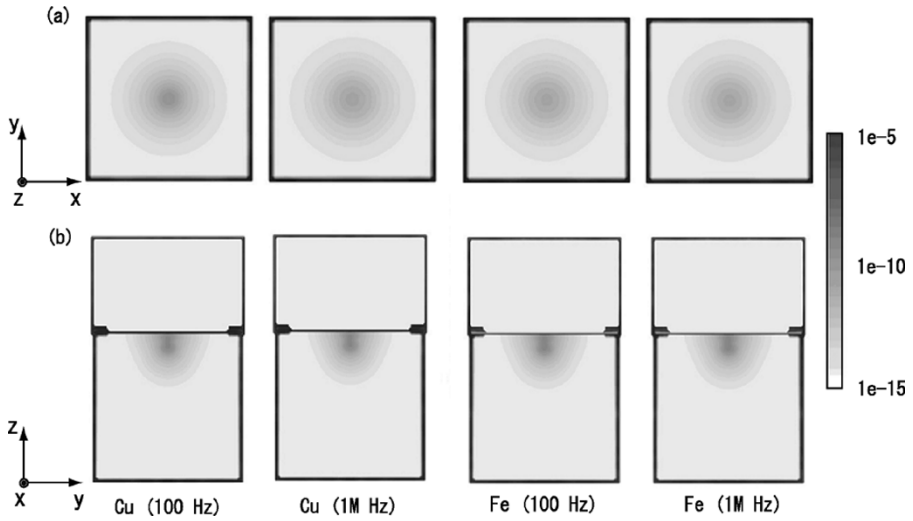

Fig. 2. Simulation of influence of shield box. The gray scale shade expresses magnetic flux density in Tesla [T]. (a) expresses magnetic flux density at horizontal points that include the plane of the loop antenna (cut at $z = 238\ \mathrm{mm}$). (b) expresses magnetic flux density at middle of shield box (cut at $x = 131\ \mathrm{mm}$).

it also includes both the spatial and the frequency domains. To estimate the accuracy within the frequency range (less than 1 MHz), we compare calculating a magnetic field from MAFIA with using the Biot–Savart's law. The magnetic field which is calculated from MAFIA is less than 0.5% different from the value generated using the Biot–Savart's law. For the commercial software we used, the number of cells is 10 M, the cell sizes are 0.1 mm (test material) to 20 mm (outside the shield box), the spatial boundary conditions for the numerical analysis are open, and the source is assumed to be a loop antenna.

Fig. 2 shows the magnetic flux density adjacent to a magnetic dipole source in the shield box. We simulate four cases. We use the nonmagnetic material Cu and ferromagnetic material Fe. These materials are placed between the lower and the upper part of the box at $z = 268\ \mathrm{mm}$. We simulate 100 Hz and 1 MHz transmissions for each of these materials. The coordinates x, y and z in Fig. 2 correspond to the coordinates of the shield box shown in Fig. 1. The magnetic flux density at the source center is 3.1×10^{-6} [T]. The magnetic flux density at the surface of the side plane of the shield box is 1×10^{-15} [T] or less. If that wave is observed at the receiver it would be much smaller than a direct wave emitted from the source, because the transmitted signal that returns through the side plane would be attenuated even more. From this figure we find that no waves reach the side of the shield box and no waves go outside of the shield box. This means that we should be able to ignore the influence of the side panels and the end panels.

To confirm the results of the above simulation, we needed to find that most all of the magnetic flux density was emitted to the testing material. If the transmitted signal observed at the receiver point includes that reflected from the side panels, we can not accurately find the SE. We measured the SE of various sizes of square sections for four materials to evaluate the magnetic flux density emitted to the material. We used nonmagnetic materials, aluminum (Al) and lead (Pb), and ferromagnetic materials, iron (Fe) and nickel (Ni). The purity of these materials was more than 99.95%. Therefore, these are isotropic materials, and there are no hard axis and easy axis. Fig. 3 shows

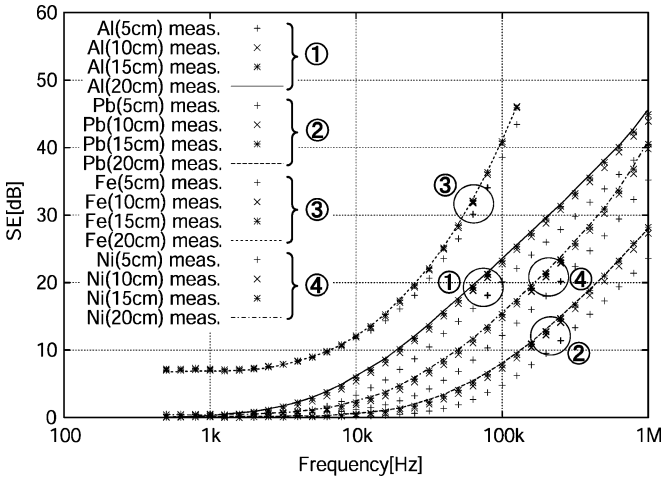

Fig. 3. SE variation as a function of type and area of shielding. The distance from the transmitter to the receiver is 20 mm.

experimentally the effect that the type and the difference of the area of the shielding material have on SE. The distance from the transmitter to the receiver is 20 mm. If the distance from the transmitter to the receiver becomes larger, the difference between the calculated value and the measured value is larger because of the reflected wave from the upper plane of the shield box. Therefore, we made the distance from the transmitter to the receiver as short as possible. The numbers which are enclosed in parentheses show the lengths of one side of the square materials. These materials were placed on several types of jigs made of 5-mm Cu plate with different size square openings. When the length of the side of the square of shielding material is increased from 50 to 100 mm, both the nonmagnetic materials and the ferromagnetic materials show about a 5-dB increase in SE. As we continue enlarging the area of the testing material, we see that SE approaches a constant value. The values are not different for the materials larger than 150 mm by 150 mm, and we find that there is no effect of reflected waves from the side of the shield box because the SE of a 200 mm $\times$ 200 mm piece of each type of shielding material is not different from the SE of a 150 mm $\times$ 150 mm piece of the same type.

From the results described above, most of the magnetic fields from the transmitter are emitted in the direction toward the testing material and no magnetic fields are emitted out of the directions of the side planes. Thus, we can ignore the influence of the circumference of the shield box.

III. Method of Electromagnetic Analysis

In calculating an electromagnetic field, we have to consider the location of the observation point, because the calculations of an electromagnetic field for a near-field point and that for a distant point are quite different. If the distance z from the observation point to a source is $z \gg \lambda/2\pi$, where λ is the wavelength, the radiation field becomes dominant and can be regarded as a plane wave. For such a case, the SE of the testing material is not related to the position of the source. But if the distance of the source from the observation point is $z \ll \lambda/2\pi$, it can not be assumed that the radiation field is the wave emitted from the source. Thus, it is necessary to calculate the electromagnetic field of a near source when calculating SE.

In order to determine the electromagnetic field more accurately, we have to increase the number of grids used in the MAFIA simulation. This requires more memory and more time in computation. For this reason, we used the Sommerfeld integral that expresses a spherical wave as a composition of cylindrical waves. Then we do a numerical analysis of a multilayered material model.

A. Boundary Condition

When the electric dipole in the Helmholtz equation is replaced with a magnetic dipole, the electromagnetic field is expressed by (2) and (3) by using a magnetic Hertz vector Π_m. Equation (4) shows the magnetic Hertz vector Π_m related to the magnetic dipole

$$E = -j\omega\mu\nabla \times \Pi_m \tag{2}$$

$$H = \nabla\nabla \cdot \Pi_m + k^2\Pi_m \tag{3}$$

$$\Pi_m = \frac{nSI}{4\pi}\frac{e^{-jkR}}{R}i_z. \tag{4}$$

Here, E is the electric field, H is the magnetic field, j is complex, ω is the angular frequency, μ is the magnetic permeability, k is wave number, n is the number of turns of the source loop current, S is the loop area, I is the loop current, R is the distance from the source, and i_z is the unit vector of z. For numerical analysis, we use the same parameters as used for the measurements.

Then the boundary conditions between the layers i and $i+1$ on the $x-y$ plane can be expressed as in (5) and (6) by applying the continuity of the H_r and E_θ component to (2) and (3), where the $x-y$ plane is the horizontal element in Cartesian coordinates

$$\frac{\partial \Pi_{m,i}}{\partial z} = \frac{\partial \Pi_{m,i+1}}{\partial z} \tag{5}$$

$$\mu_i \Pi_{m,i} = \mu_{i+1}\Pi_{m,i+1}. \tag{6}$$

Here, the Hertz vectors for layer i and for layer $i+1$ are expressed as $\Pi_{m,i}$ and $\Pi_{m,i+1}$.

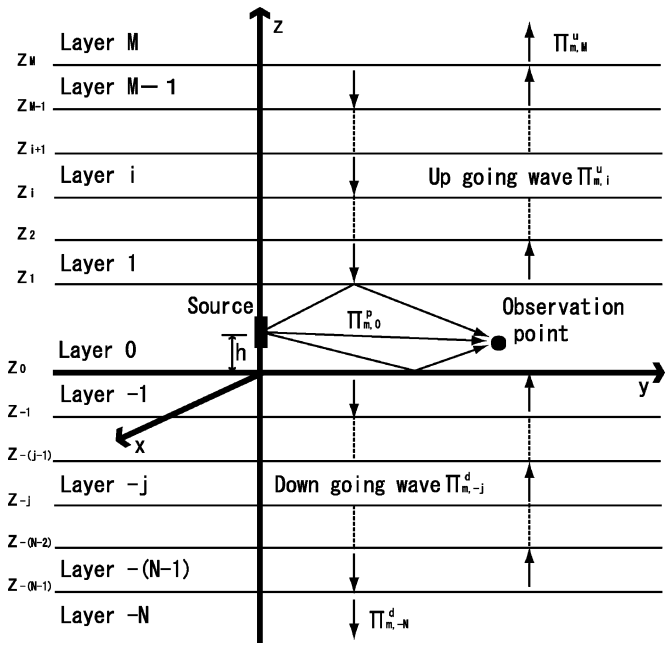

Fig. 4. Multilayered model.

B. Electromagnetic Analysis by Using a Multilayered Model

The coordinate system of the multilayered model which we use to calculate the electromagnetic field is shown in Fig. 4. A magnetic dipole source is assumed at $z = h$ with homogeneous layers above and below the dipole extending to infinity in the horizontal directions. The axial direction of the dipole source is located vertically perpendicular to each layer. The Hertz vector for the up-going wave is expressed as $\Pi^u_{m,i}$, the Hertz vector for the down-going wave is expressed as $\Pi^d_{m,i}$, and the Hertz vector for the direct wave is expressed as $\Pi^p_{m,i}$, where the subscript i indicates the layer. The Hertz vector in layer i is expressed by (7). By using the Sommerfeld integral representation to express a spherical wave by the synthesis of cylindrical waves, (4) can be transformed into (8) for the up-going waves and into (9) for the down-going waves in layer i

$$\Pi_{m,i} = \Pi^u_{m,i} + \Pi^d_{m,i} \tag{7}$$

$$\Pi^u_{m,i} = \frac{nSI}{4\pi}\int_0^\infty f^u_{m,i}(\lambda)J_0(\lambda r)e^{-\nu_i(z-z_i)}\lambda d\lambda \tag{8}$$

$$\Pi^d_{m,i} = \frac{nSI}{4\pi}\int_0^\infty f^d_{m,i}(\lambda)J_0(\lambda r)e^{\nu_i(z-z_i)}\lambda d\lambda \tag{9}$$

where

$$\nu_i = \sqrt{\lambda^2 - k_i^2}.$$

The integrand elements $f^u_{m,i}$ and $f^d_{m,i}$ are unknown functions of the integration variable λ with the subscripts and superscripts the same as for Π_m. In Appendix III we describe how these elements are determined. Here, J_0 is a zero-order Bessel function of the first kind, r is the radial distance in cylindrical coordinates, and z_i is the distance of layer i along the z-axis.

Then we substitute the Hertz vectors [from (8) and (9)] into the boundary conditions (5) and (6) in order to solve for the unknown functions $f^u_{m,i}$, $f^d_{m,i}$. This expresses the results as a

known 2×2 matrix including a_{11}, a_{12}, a_{21}, a_{22} as shown in (10) at the bottom of the page.

Then expanding from layer 0 to layer M, (10) can be transformed to the following:

$$\begin{pmatrix} f^u_{m,0} \\ f^d_{m,0} \end{pmatrix} = \prod_{i=0}^{M-1} \begin{pmatrix} A_{11} & A_{12} \\ A_{21} & A_{22} \end{pmatrix} \begin{pmatrix} f^u_{m,M} \\ 0 \end{pmatrix} - \frac{1}{\nu_0} \begin{pmatrix} e^{\nu_0 h} \\ 0 \end{pmatrix}. \tag{11}$$

Here, A_{11}, A_{12}, A_{21}, A_{22} are components of the known matrix, and h is the distance from the origin.

Similarly, expanding from layer 0 to layer $-N$ using boundary conditions, we calculate the Hertz vectors for layer 0 to $-N$ of the matrix below the source. We are able to find the unknown parameters by solving the equality for layer 0 for the two cases. Using these derived unknown matrices, we can calculate the electromagnetic field in arbitrary layer i.

We used the Sommerfeld integral which expresses a spherical wave by composition of cylindrical waves, and for the numerical calculation we used the trapezoidal rule on the real axis. Since the integral converges as the numerical calculation proceeds, the processing is terminated as soon as the integrated value does not change. We find using this method to be very effective, because results of comparing e^{-jkR}/R with the Sommerfeld integral are very close up to the eighth decimal place. Therefore, we are able to validate our method.

IV. Estimation of Relative Permeability and Conductivity

In our electromagnetic field analysis, we replace the shield box with homogeneous multilayer infinite plane plates described in Section III and estimate the relative permeability and conductivity. However, the shield box is not horizontally infinite, and it has limited dimensions. Therefore, we experimentally measured the differences due to the type and area of shielding in Section II, and found that nearly all of the magnetic field is emitted into the test material. Thus the calculations using the infinite plane assumption are valid for comparison with our measurements.

In order to estimate the relative permeability and the conductivity, we first measured SE with the shield box. Then we estimate the relative permeability and the conductivity by adjusting these electric parameters in order to get the calculated values of the SE close to the measured values.

A. SE Calculations Using Nominal Electric Parameters

The SE calculations are most influenced by the electric parameters. SE has different characteristics as a function of frequency for different types of materials, and characteristic curves can be drawn for each type. Fig. 5 shows the calculated and measured values of SE for three nonmagnetic (Al, Pb, Cu) and two ferromagnetic (Ni, Fe) test materials.

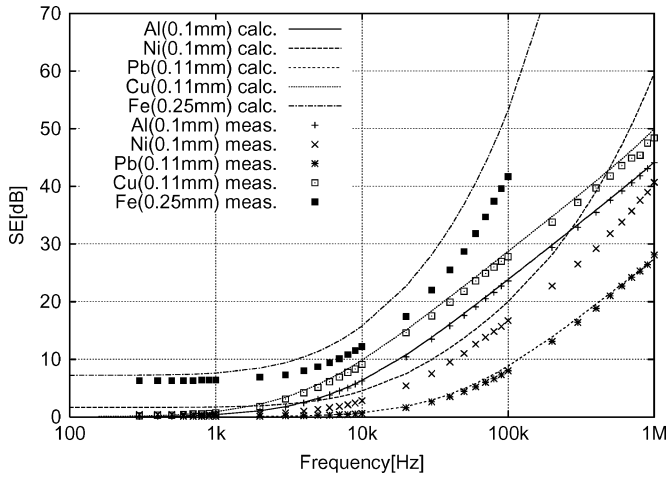

Fig. 5. SE for three nonmagnetic (Al, Pb, Cu) and two ferromagnetic (Ni, Fe) test materials. The lines show the calculated values obtained by using the nominal values of the electric parameters and the symbols show the measured values. These areas are 250 mm squares. The numbers enclosed in parenthesis are the thicknesses of the test materials.

Here, the nominal values of the electric parameters are used for calculating the SE. In the case of the nonmagnetic materials, the experimental values and analytical values of SE are very close at all frequencies. But in the case of the ferromagnetic materials, as the frequency becomes high, the calculated SE becomes much larger than the measured SE. We see that the calculated SE of the ferromagnetic shielding materials coincides with the measured values only at the low frequencies.

B. The Estimation Method

In the multilayered model, we used a boundary condition for each layer and calculated an electromagnetic field near the source. When the estimation of relative permeability and conductivity technique is used, the parameters are determined by bringing SE close to the experimental values. In this study, the least squares method is used as the method to get close to the experimental values. The electric parameters are changed in order, and the difference between the squares of the analytic values and the squares of the experimental values is made as small as possible. When the difference of the squares of the calculated and measured values is at a minimum, the SE is at its estimation value. For estimation of electric parameters, first we determine the conductivity, and next change the relative permeability. When we first determine the relative permeability, the estimated values become the same. Even if we change the initial values, estimated results do not change.

$$\begin{aligned} \begin{pmatrix} f^u_{m,i} \\ f^d_{m,i} \end{pmatrix} &= \frac{1}{2\mu_i\nu_i} \begin{pmatrix} (\mu_i\nu_{i+1} + \mu_{i+1}\nu_i)e^{\nu_i(z_i - z_{i-1})} & (-\mu_i\nu_{i+1} + \mu_{i+1}\nu_i)e^{\nu_i(z_i - z_{i-1})} \\ (-\mu_i\nu_{i+1} + \mu_{i+1}\nu_i)e^{-\nu_i(z_i - z_{i-1})} & (\mu_i\nu_{i+1} + \mu_{i+1}\nu_i)e^{-\nu_i(z_i - z_{i-1})} \end{pmatrix} \begin{pmatrix} f^u_{m,i+1} \\ f^d_{m,i+1} \end{pmatrix} \\ &\equiv \begin{pmatrix} a_{11} & a_{12} \\ a_{21} & a_{22} \end{pmatrix} \begin{pmatrix} f^u_{m,i+1} \\ f^d_{m,i+1} \end{pmatrix}. \end{aligned} \tag{10}$$

C. Transmitter Current

So far, this system has not been able to estimate the electric parameters for ferromagnetic material, because the calculated SE was not in agreement with the measured value in the frequency range of interest. We considered as one of the causes that the transmitter current possibly changed. In fact, for ferromagnetic materials close to the loop antenna, their inductance should change. If the inductance changes, the loop antenna's current might also change.

Therefore, we measured the transmitter's current. For measurement, we used a 250 mm by 250 mm piece of test materials, and the distance from the transmitter to the receiver was 20 mm. But we found no change in the transmitter current that would cause the difference in the calculated and measured values of SE for ferromagnetic materials.

D. Measurement of Relative Permeability Using the $B-H$ Curve Method

After determining that there was no relation to current, we then considered taking into account the frequency characteristics of the permeability of the materials.

Since most of the data of relative permeability available in textbooks are for dc, we have to evaluate their nominal ac values by generating them ourselves. The magnetic field H and magnetic flux density B are related as $B = \mu H$. Our method to determine the nominal values for the ac case is to measure the relative permeability as a function of frequency using $B-H$ curves.

We first made a toroidal core out of the testing material and then wound two wire coils with 10–20 turns each around the core. Then we generated a magnetic field with the first coil and measured the magnetic flux density on the second coil. The relative permeability was determined from the slope of the resultant $B-H$ curve.

In this process, we used the same level of magnetic field as that emitted from the transmitting antenna of the shield box to determine the relative permeability. The determined relative permeability was then compared to the value derived from the SE calculation.

E. Consideration of Frequency Characteristics

Our next step was to reduce the difference between the calculated SE values and the measured SE values considering the frequency characteristics of the relative permeability.

In the low frequency range, we found the calculated values and the measured values of SE even for the ferromagnetic materials to be quite similar. We used this fact to take the frequency characteristics into account. In the low frequency range for each material where the calculated and measured values are in closest agreement, we first used the least squares method to estimate a relative permeability and conductivity without frequency dependence. We then used the derived conductivity as a constant and at each measurement frequency varied only the relative permeability to minimize the difference in SEs. This process of finding at a given frequency the calculated SE that comes closest to the SE measured in the shield box yields the conductivity independent of frequency and the relative permeability as a function of frequency.

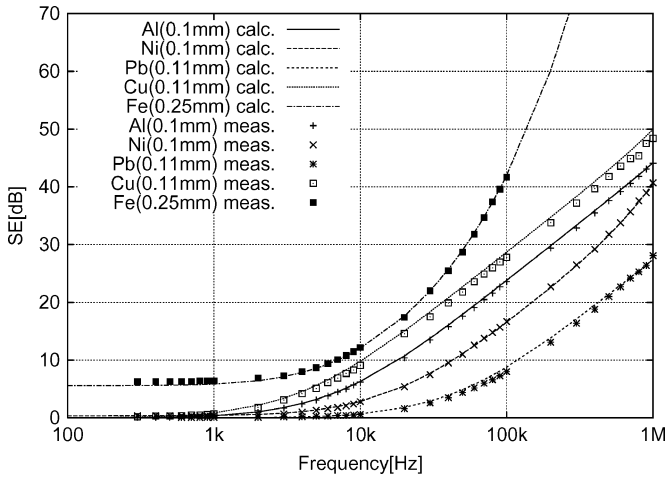

Fig. 6. SE comparison with frequency characteristics of the electric parameters taken into account.

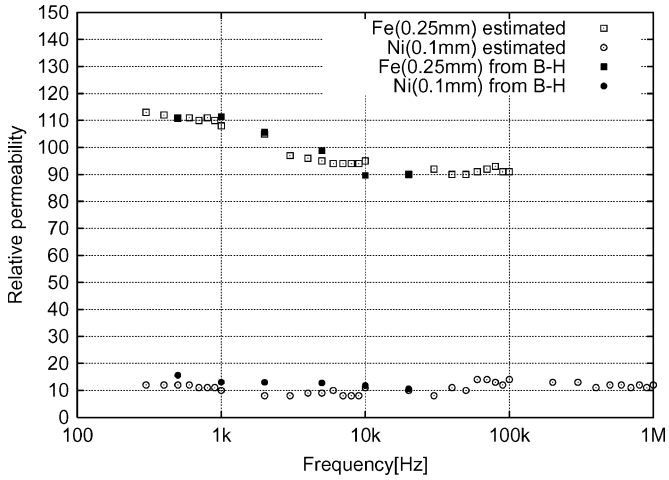

Fig. 7. Frequency characteristics of the relative permeability.

V. Result of Estimation

We tested the estimation technique of electric parameters by using materials with the known electric parameters for the dc case. In this research, we varied the electric parameters μ_r(relative permeability) and σ(conductivity) in the SE calculations in order to get the best fit with the measured values. The results are shown in Fig. 6. The least squares fitting process determines the relative permeability and conductivity. Fig. 7 shows the frequency characteristics of the relative permeability for the ferromagnetic materials. Hysteresis is very low. Therefore, our numerical analysis uses only the real part of μ, and we did not consider the imaginary part of μ_r. The open squares show the relative permeability of Fe that was estimated by our method. The open circles show the relative permeability of Ni that was estimated by our method. The filled squares show the relative permeability of Fe that was determined from the $B-H$ curve. The filled circles show the relative permeability of Ni that was determined from the $B-H$ curve. The values for the nonmagnetic materials are not plotted here, since they were

TABLE I
NOMINAL ELECTRIC PARAMETER VALUES COMPARED TO ESTIMATED VALUES. RELATIVE PERMEABILITY OF Fe AND Ni ARE AT 1 KHz

Materials (thickness)	μ_r [nom. / cal.]	σ [S / m] [nom. / cal.]
Al (0.1 mm)	1.0 / 1.0	3.63×10^7 / 3.51×10^7
Cu (0.11 mm)	1.0 / 1.0	5.80×10^7 / 5.69×10^7
Pb (0.11 mm)	1.0 / 1.0	0.50×10^7 / 0.50×10^7
Fe (0.25 mm)	111.0 / 108.0	1.02×10^7 / 0.92×10^7
Ni (0.1 mm)	13.0 / 10.0	1.45×10^7 / 1.39×10^7

always equal to 1.0. The relative permeability derived from our SE analysis and that calculated from our $B-H$ curve testing are similar.

Table I compares the nominal values of the relative permeability and conductivity with those estimated from this method. For the nonmagnetic materials, the calculated relative permeability was the same as the nominal value. The calculated conductivity was the same as the nominal value for Pb, 1.9% greater for Cu, and 3.3% greater for Al. For the ferromagnetic materials, the calculated value was 4.1% higher for Ni and 9.8% higher for Fe. For comparison, measurement of a conductivity using the four point probe method had an error rate of 20% or less. Thus, we find that our method for measuring conductivity is better than the previously existing method. The nominal values for the relative permeability of the ferromagnetic materials are close to the values derived with our $B-H$ curve testing. For Fe, the nominal and calculated values were the same for 500 Hz, 2 and 20 kHz. The estimated values were 2% higher for 1 and 5 kHz and 3% lower at 10 kHz. For Ni, the nominal and the calculated values were the same at 10 and 20 kHz. The estimated values at the lower frequencies were 20% to 33% lower than the nominal values.

VI. CONCLUSION

We have investigated the estimation of relative permeability and conductivity by measuring SE by using a shield box and comparing the results with the calculated SE which is a function of the conductivity and relative permeability. Because we had a near-field source, we used the Sommerfeld integral that expresses spherical waves by composition of cylindrical waves. The Sommerfeld integral can only be used for an infinite plane plate, but the dimensions of the shield box are limited. Therefore, we evaluated the influence of the circumference of the shield box. From simulation and measurement, we found that there was no influence.

Using the estimation method, we found that the SE values calculated using the nominal values for the electric parameters and the measured SE values were different. After eliminating the possibility of changes in transmitter current as a cause for the difference, we considered the frequency characteristics of the electric parameters as the cause of the difference. In the low frequency region where the calculated and measured SE values were close, we used the estimation method to determine the conductivity which does not change with frequency. Using the conductivity as a constant, we then varied the relative permeability to find the minimum value of the difference. In this way we could estimate conductivity and relative permeability with frequency characteristics. In the shield box method, as the frequency becomes higher, the SE becomes higher too. Then there is not enough dynamic range for the measurements, and we therefore can not estimate the electric parameters in the high frequency range. In this paper, we focus on the low frequency range.

Hereafter, the estimation of relative permeability and conductivity, for not only nonmagnetic material but also for ferromagnetic material, is attainable. This method will be useful for the design of electromagnetic shielding sheets.

APPENDIX I
CALCULATION OF THE ELECTROMAGNETIC FIELDS IN EACH LAYER

The Hertz vector defined by (4) is substituted into (2) and (3). Then the electromagnetic field in layer i is calculated as shown below from the layers both above and below the source

$$\begin{aligned} E_{\theta,i} &= -j\omega\mu_i\frac{\partial \Pi_{m,i}}{\partial r} \\ &= -\frac{j\omega\mu_i nSI}{4\pi}\int_0^\infty J_1(\lambda r) \\ &\quad\times\left(f^u_{m,i}e^{-\nu_i(z-z_{i-1})}+f^d_{m,i}e^{\nu_i(z-z_{i-1})}\right)\lambda^2 d\lambda \quad (12) \\ H_{r,i} &= \frac{\partial^2}{\partial r\partial z}\Pi_m \\ &= \frac{nSI}{4\pi}\int_0^\infty \nu_i J_1(\lambda r) \\ &\quad\times\left(f^u_{m,i}e^{-\nu_i(z-z_{i-1})}-f^d_{m,i}e^{\nu_i(z-z_{i-1})}\right)\lambda^2 d\lambda \quad (13) \\ H_{z,i} &= \left(k_i^2\Pi_{m,i}+\frac{\partial^2}{\partial z^2}\Pi_{m,i}\right) \\ &= \frac{nSI}{4\pi}\int_0^\infty \left(k_i^2+\nu_i^2\right)J_0(\lambda r) \\ &\quad\times\left(f^u_{m,i}e^{-\nu_i(z-z_{i-1})}+f^d_{m,i}e^{\nu_i(z-z_{i-1})}\right)\lambda d\lambda. \quad (14) \end{aligned}$$

The electromagnetic field in layer 0 which contains the source is calculated as shown below. For the variable sign exponent, the upper sign is used for the layers above the source and the lower sign is used for the layers below the source

$$\begin{aligned} E_{\theta,0} &= -\frac{j\omega\mu_0 nSI}{4\pi}\int_0^\infty J_1(\lambda r) \\ &\quad\times\left(f^u_{m,0}e^{-\nu_0 z}+f^d_{m,0}e^{\nu_0 z}+\frac{1}{\nu_0}e^{\mp\nu_0(z-h)}\right)\lambda^2 d\lambda \quad (15) \\ H_{r,0} &= \frac{nSI}{4\pi}\int_0^\infty \nu_0 J_1(\lambda r) \\ &\quad\times\left(f^u_{m,0}e^{-\nu_0 z}-f^d_{m,0}e^{\nu_0 z}+\frac{1}{\nu_0}e^{\mp\nu_0(z-h)}\right)\lambda^2 d\lambda \quad (16) \\ H_{z,0} &= \frac{nSI}{4\pi}\int_0^\infty \left(k_0^2+\nu_0^2\right)J_0(\lambda r) \\ &\quad\times\left(f^u_{m,0}e^{-\nu_0 z}+f^d_{m,0}e^{\nu_0 z}+\frac{1}{\nu_0}e^{\mp\nu_0(z-h)}\right)\lambda d\lambda. \quad (17) \end{aligned}$$

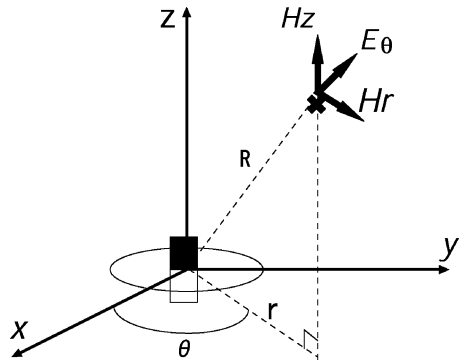

Fig. 8. Coordinate system for radiation emitted from a magnetic dipole source in free space.

APPENDIX II
CALCULATION OF THE EMITTED RADIATION FROM A MAGNETIC DIPOLE

In free space, a loop antenna with n turns in the $x-y$ plane with area S and current I is placed at the origin in the (r,θ,z) coordinate system. The emitted electromagnetic field is expressed as shown below. Here, $R=\sqrt{z^2+r^2}$ where z is the height of the observation point above the loop antenna plane. Fig. 8 shows the electromagnetic field emitted from the source

$$E_\theta = -\frac{j\omega\mu nSI}{4\pi}\left(\frac{1}{R^3}+j\frac{k}{R^2}\right)e^{-jkR} \tag{18}$$

$$H_r = \frac{nSI}{4\pi}\left(-\frac{k^2rz}{R^3}+j\frac{3rzk}{R^4}+\frac{3rz}{R^5}\right)e^{-jkR} \tag{19}$$

$$H_z = \frac{nSI}{4\pi}\left(\frac{3z^2}{R^5}+j\frac{3kz^2}{R^4}-\frac{1+k^2z^2}{R^3}-j\frac{k}{R^2}+\frac{k^2}{R}\right)e^{-jkR}. \tag{20}$$

APPENDIX III
DERIVATION OF SE USING NUMERICAL ANALYSIS

We first calculate the Hertz vector in layer i, (7), for all of the layers. We then apply the boundary conditions, (5) and (6), for each boundary between layers and calculate the unknown coefficients f_m^u and f_m^d. We then substitute the coefficients into (12)–(17), and calculate the electromagnetic fields for each layer. To determine H_1 in (1), we calculate the magnetic field at the layer in which the receiving antenna is located. H_0 in (1) is calculated by using (20) for the position where the observation point exists.

SE is calculated from the ratio of H_0 to H_1 at the observation point.

ACKNOWLEDGMENT

The authors would like to thank Prof. R. R. Anderson at Kanazawa University in Japan (now at the University of Iowa) and Prof. S. Yamada at Kanazawa University for their valuable comments and suggestions.

REFERENCES

[1] Y. Shimizu and A. Sugiura, "Incidence and obstacle of electromagnetic interference wave," *Nikei Gijyutsu Tokyo*, pp. 3–18, Sep. 1999.
[2] Guideline for limiting exposure to time-varying electric, magnetic, and electromagnetic fields (up to 300 GHz), Int. Commission on Non-Ionizing Radiation Protection, Apr. 1998.
[3] Y. Shimizu and A. Sugiura, "Incidence and obstacle of electromagnetic interference wave," *Nikei Gijyutsu Tokyo*, p. 209, Sep. 1999.
[4] T. Tsuchikawa, J. Wang, and O. Fujiwara, "FDTD Simulation of shielding effectiveness of metal plated plastics for information terminals," Tech. Rep. IEICE, EMCJ2001-86, Nov. 2001.
[5] Y. Yoshimura, I. Nagano, S. Yagitani, T. Ueno, and T. Nakayabu, "Electromagnetic shielding effectiveness of a multilayered medium in the vicinity of a dipole source," *IEEJ Trans. Fundamentals Materials*, vol. 121, no. 2, pp. 169–176, Feb. 2001.
[6] *Methods of Measurement of the Magnetic Properties of Electrical Steel Sheet and Strip by Means of an Epstein Frame*, Int. Standard, CEI/IEC 60 404-2, Mar. 1996.
[7] *Method of Measurement of Magnetic Properties of Magnetic Steel Sheet and Strip at Medium Frequencies*, Int. Standard, CEI/IEC 60 404-10, Aug. 1988.
[8] I. Nagano, Y. Yoshimura, S. Sagitani, H. Yokomoto, T. Tosaka, and T. Nakayabu, "Estimation of electric parameters of thin electromagnetic shielding materials," *IEEJ Trans. Fundamentals Materials*, vol. 123, no. 2, pp. 192–199, Feb. 2003.
[9] I. Nagano, "Radio waves in an inhomogeneous medium," *Hosyu Syuppan*, pp. 12–42, Jan. 1977.
[10] F. M. Tesche, M. V. Ianoz, and T. Karlsson, *EMC Analysis Methods and Computational Models*. New York: Wiley-Interscience, 1997, pp. 550–552.
[11] W. H. Hayt Jr, *Engineering Electromagnetics*. New York: McGraw-Hill, 1981, p. 430.
[12] D. Jiles, *Introduction to Magnetism and Magnetic Materials*, 2 ed. London, U.K.: Chapman & Hall, 1998, pp. 91–96.
[13] MAFIA Release 4.00, Gesellschaft für Computer-Simulationstechnik m.b.H., 1997.

Toshihide Tosaka (S'04) received the B.E. and the M.E. degrees in computer science from Nihon University, Fukushima, Japan, in 2000 and 2002, respectively. Since 2002, he has been working toward the Ph.D. degree at Kanazawa University, Ishikawa, Japan.

He is engaged in electromagnetic interference/compatibility (EMI/EMC) problems.

Mr. Tosaka is a Member of the Institute of Electronics, Information and Communication Engineers (IEICE) of Japan.

Isamu Nagano received the B.E. and M.E. degrees from Kanazawa University, Ishikawa, Japan, in 1968 and 1970, respectively, and the Ph.D. degree in electrical engineering from Kyoto University, Kyoto, Japan, in 1980.

Since 1970, he has been with Graduate School of Natural Science and Technology, Kanazawa University, where he is now a Professor of radio wave science and engineering. From 1983 to 1984, he was an NRC Resident Research Associate at NASA Jet Propulsion Laboratory. His research fields are the theoretical and experimental studies of electromagnetic wave propagation in geospace using rocket and satellites, and of EMI/EMC problems.

Dr. Nagano is a Member of the Institute of Electronics, Information and Communication Engineers (IEICE) of Japan, the Institute of Electrical Engineers (IEE) of Japan, the Society of Geomagnetism and Earth, Planetary and Space Sciences (SGEPSS) of Japan, and the American Geophysical Union (AGU). He was awarded the *Tanakadate* Prize in 1987, the NASA Group Achievement Award in 1998, and the *Hokkoku Bunka* Prize in 2000.

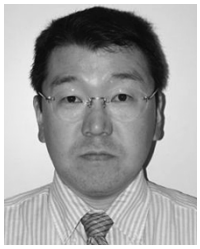

Satoshi Yagitani received the B.E., M.E., and Ph.D. degrees in electrical and computer engineering from Kanazawa University, Ishikawa, Japan, in 1988, 1990 and 1993, respectively.

Since 1993, he has been with Graduate School of Natural Science and Technology, Kanazawa University, where he is now an Associate Professor of radio wave science and engineering. From 1997 to 1998, he was a Visiting Researcher at the University of Minnesota, Crookston. His research interests are plasma wave propagation in geospace, the analysis of wave field data obtained by satellites, and EMI/EMC problems.

Dr. Yagitani is a Member of the Institute of Electronics, Information and Communication Engineers (IEICE) of Japan, the Society of Geomagnetism and Earth, Planetary and Space Sciences (SGEPSS) of Japan, and the American Geophysical Union (AGU). He was awarded the *Sangaku Renkei Suishin Ishikawa (Shourei)* Prize in 2001.

Yoshiyuki Yoshimura received the B.E. and M.E. degrees in mechanical systems engineering from Nagaoka University of Technology, Niigata, Japan, in 1988 and 1990, respectively, and the Ph.D. degree from Kanazawa University, Ishikawa, Japan, in 2003.

Since 1990, he has been with the Product and Technology Department, Industrial Research Institute of Ishikawa, where he is now a Researcher. He is engaged in electromagnetic interference/compatibility (EMI/EMC) problems.

Dr. Yoshimura is a Member of the Institute of Electronics, Information and Communication Engineers (IEICE) of Japan and the Institute of Electrical Engineers (IEE) of Japan